



**HAL**  
open science

# Crystallinity and Molecular Packing of Small Molecules in Bulk-Heterojunction Organic Solar Cells

Emilio Palomares, Laurent Billon, Aurelien Viterisi

► **To cite this version:**

Emilio Palomares, Laurent Billon, Aurelien Viterisi. Crystallinity and Molecular Packing of Small Molecules in Bulk-Heterojunction Organic Solar Cells. *Applied Sciences*, 2022, 12 (11), pp.5683. 10.3390/app12115683 . hal-03767013

**HAL Id: hal-03767013**

**<https://univ-pau.hal.science/hal-03767013>**

Submitted on 1 Sep 2022

**HAL** is a multi-disciplinary open access archive for the deposit and dissemination of scientific research documents, whether they are published or not. The documents may come from teaching and research institutions in France or abroad, or from public or private research centers.

L'archive ouverte pluridisciplinaire **HAL**, est destinée au dépôt et à la diffusion de documents scientifiques de niveau recherche, publiés ou non, émanant des établissements d'enseignement et de recherche français ou étrangers, des laboratoires publics ou privés.

Review

# Crystallinity and Molecular Packing of Small Molecules in Bulk-Heterojunction Organic Solar Cells

Emilio Palomares , Laurent Billon  and Aurelien Viterisi \* 

The Institute of Analytical Sciences and Physico-Chemistry for Environment and Materials (IPREM), Technopole Hélioparc, 2 Avenue du Président Pierre Angot, CEDEX 09, 64053 Pau, France; epalomares@icq.es (E.P.); laurent.billon@univ-pau.fr (L.B.)

\* Correspondence: aurelien.viterisi@univ-pau.fr

**Abstract:** Crystallinity has played a major role in organic solar cells (OSCs). In small molecule (SM) bulk-heterojunction (BHJ) OSCs, the crystallinity and crystalline packing of SM donors have been shown to have a dramatic impact on the formation of an optimum microstructure leading to high-power conversion efficiency (PCE). Herein we describe how crystallinity differs from polymers to SMs, and how the packing habits of SMs (particularly donors) in active layers of BHJ devices can be described as following two different main modes: a single crystal-like and a liquid crystal-like packing type. This notion is reviewed from a chronological perspective, emphasising milestone donor structures and studies focusing on the crystallinity in SM-BHJ OSCs. This review intends to demonstrate that a shift towards a liquid crystalline-like packing can be identified throughout the history of SM-BHJ, and that this shift can be associated with an increase in overall PCE.

**Keywords:** organic solar cell; photovoltaics; small molecule; bulk heterojunction; crystallinity; crystalline packing



**Citation:** Palomares, E.; Billon, L.; Viterisi, A. Crystallinity and Molecular Packing of Small Molecules in Bulk-Heterojunction Organic Solar Cells. *Appl. Sci.* **2022**, *12*, 5683. <https://doi.org/10.3390/app12115683>

Academic Editor: Fabrice Goubard

Received: 1 April 2022

Accepted: 30 May 2022

Published: 3 June 2022

**Publisher's Note:** MDPI stays neutral with regard to jurisdictional claims in published maps and institutional affiliations.



**Copyright:** © 2022 by the authors. Licensee MDPI, Basel, Switzerland. This article is an open access article distributed under the terms and conditions of the Creative Commons Attribution (CC BY) license (<https://creativecommons.org/licenses/by/4.0/>).

## 1. Introduction

For several decades, the manufacture high-efficiency photovoltaics (PVs) was thought to be possible only from solid-state semiconductor materials of ordered (crystalline) nature, having high dielectric constants and high electron and hole mobilities. For that purpose, extremely pure crystalline mono- or polycrystalline silicon has proved to be the material of choice for PV solar cell manufacture. The discovery of the semiconducting properties of conjugated polymers by Heeger, MacDiarmid and Shirakawa has established a new paradigm in semiconductor physics, which eventually led to the development of organic solar cells in the late 1980s. Although the first organic planar heterojunction solar cell was reported by Tang and co-workers in 1986 [1], organic solar cells (OSCs) only began to attract significant interest after the demonstration of PCE over 2% in solution-processed polymer-fullerene bulk-heterojunctions with polyphenylenevinylene electron donors: MEH-PPV or MDMO-PPV. These types of solar cells showed, contrary to early expectations, that efficient photovoltaic devices could be manufactured with semiconductors having rather distinct features from inorganic semiconductors. Indeed, the components of the so-called active layer are very disordered with respect to their inorganic counterparts, and as a consequence, hole and electron mobility, as well as dielectric constants, are generally three to four orders of magnitude lower than those of silicon. Despite these apparent conundrums, great efforts made by the scientific community over the last decades proved that organic solar cells with an efficiency of a similar magnitude to those of silicon-based PV could be manufactured on the laboratory scale. These achievements were made possible by several breakthroughs in research areas as diverse as polymer chemistry, semiconductors physics and physical chemistry. Consequently, the underlying mechanisms of OSCs are currently reasonably well understood [2,3]. However, the extent to which the characteristics of a device can be predicted according to the chemical structure of its active layer components is still limited. The

reason behind it lies in the fact that the morphology (or microstructure) of the photoactive layer of OSCs is the key determinant of the overall device's characteristics [4–14]. Phase segregation into domains of donors and acceptors and crystallinity are essential features. The latter properties are challenging to predict, considering the sole chemical structure of the electron donor (D) and electron acceptor (A) components. In the case of small-molecule (SM) bulk-heterojunction (BHJ) OSCs in particular, the crystalline properties of the D and A molecules are critical to the device function since the formation of segregated D/A domains relies on the formation of crystalline domains of pure donor and pure acceptor. The kinetics and thermodynamics of the crystallisation process are likely the primary physical parameter involved in the genesis of the microstructure [15–19]. The recent progress in the field, with record PCEs over 14% using non-fullerene acceptors (NFA) [20], demonstrates the importance of understanding the evolution of the crystallinity of the active layer from a fundamental perspective.

Therefore, herein we describe the evolution of the crystalline properties of active layers in SM-BHJ OSCs from a historical perspective. We will first briefly introduce the concept of crystallinity in the context of polymers, liquid crystals and small molecules, and then review the methods currently used to characterise the crystallinity of SM-BHJ active layers. Next, the crystalline characteristics of the main classes of donor/acceptors blends will be reviewed, particularly focusing on the different modes of molecular packing in crystalline films of OSC active layers. We show that, throughout the evolution of the SM-BHJ field, SMs shifted from a single-crystalline-like to liquid-crystalline-like packing habit in active layers of OSCs. We believe that such a shift is directly linked with the trend in the design of SMs (D or A) consisting—in a broad sense—of adding a large proportion of alkyl chains to the conjugated core (far beyond the necessary amount for solubility). This trend is likely to have significantly contributed to the increase in PCEs in SM-BHJ OSCs, as we will show herein.

## 2. Crystallinity in Active Layers of OSCs

In the early days of OSCs, active layers of polymer-based solar cells were thought of being primarily amorphous. However, the introduction of thiophene-based conjugated polymers, such as poly(3-hexylthiophene) P3HT, demonstrated the importance of crystallinity in OSCs [21,22]. Indeed, the need for an active layer annealing, in order to achieve improved current density-voltage ( $J$ - $V$ ) characteristics, which was initially mostly linked with phase segregation, was soon associated with polymer crystallisation [23–28]. However, the concept of crystallinity for polymers is somewhat different from the crystallinity of small molecules since, in the former case, crystallinity is understood as the presence of ordered stacks of molecular fragments in an otherwise disordered matrix of polymer chains. These fragments stack over a sufficiently long range to form well-defined planes detected by X-ray diffraction, hence the association with crystallinity [29]. Although these stacks are ordered, the very nature of polymers, i.e., polydisperse mixtures of different chain lengths, limits the order and size of these domains. The condition for such stacking phenomena is the existence of relatively strong intramolecular interactions, generally,  $\pi$ - $\pi$  stacking or hydrophobic interactions favourable over long distance ranges.

Similar crystalline behaviour is observed in the case of liquid crystals, which contrary to polymers, consist of small molecules with discrete and well-defined structures. Their specific design—i.e., the extended conjugated core and long lateral alkyl chains—form ordered stacks of molecules in the mesophases (intermediate phase between crystalline and liquid phase) [30]. These disordered crystalline domains form generally from  $\pi$ - $\pi$  stacked conjugated cores or alkyl chain intramolecular interactions. Therefore, these strong intermolecular interactions limit the degree of order to a similar extent to that of polymers. That is, despite consisting of small molecules of a discrete structure, their packing in the mesophases is not expected to adopt a perfect arrangement such as that of small molecules in the solid state. Indeed, the concept of crystallinity in the case of the latter molecules is more comprehensive. The well-defined structure of the molecules, together with their

higher degrees of freedom resulting from more diverse types of weak intermolecular interactions, defines crystallinity as the perfect arrangement of molecules following Bravais lattices (from one of the 230 existing space groups) [31]. This type of packing habit is, in fact, identical to that of inorganic materials, however, the intramolecular interactions between organic molecules being weaker, the size of the crystals, i.e., the extent of the arrangement, is generally limited to small sizes compared to inorganic crystalline materials, which generally rely on strong ionic interactions.

The crystallinity of either polymers or SMs is mainly studied using X-ray diffraction, which is one of the best methods to characterise materials encompassing different degrees of crystallinity and order. Indeed, the diffraction of ordered planes following Bragg's law can give direct information on the interplane distances of specific molecule stacks for polymers and liquid crystals [32]. However, in the case of small molecules, these interplane distances must be assigned to the diffraction planes of an arrangement of the molecule in a specific Bravais lattice. This statement implies that small molecules in a crystalline state consist of a perfect arrangement of packed units in one of the 230 existing space groups in the crystalline state. The space group constituting the crystal is first determined from a collection of diffraction peaks recorded in all directions of space. The molecular packing (so-called crystal structure) in that specific space group is later retrieved from the relative intensity of the diffraction peaks via diffraction data refinement. Consequently, the molecular packing of a polycrystalline sample of a small molecule, i.e., a powder or thin-film sample, could only be determined by comparing its diffraction pattern with a calculated diffractogram from a single-crystal structure.

### 3. X-ray Diffraction Characterisation Techniques

The characterisation of thin films of active layers of solar cell devices has adapted to the materials composing the active layers of early solar cell devices, namely polymers. In the case of crystallinity, the choice of X-ray diffraction is evident, however the measuring setup must be adapted to the features of the active layers. Therefore, one of the most common X-ray diffraction systems used on the lab scale is the so-called Bragg–Brentano geometry, where the incident angle  $\omega$  is defined between the X-ray source and the sample. The diffracted angle,  $2\theta$ , is defined between the incident beam and the detector angle (Figure 1a). The incident angle  $\omega$  is always  $\frac{1}{2}$  of the detector angle  $2\theta$ . Although this setup can be used to characterise thin films, it is usually limited to films of very crystalline materials (e.g., inorganic materials such as perovskites, for example), the Bragg–Brentano geometry is generally most commonly used for crystalline powders [31,32]. The limited crystallinity of polymers—i.e., stacked polymer units over short ranges—together with the fact that OSCs' active layers are in the range of 50 to 200 nm in thickness at most, requires a deeper penetration of the X-ray beam for increased signal-to-noise ratios, since the intensity of the diffraction beam is proportional to the overall crystalline volume. In order to reach such irradiation depth, a so-called grazing incidence X-ray diffraction (GIXRD), or grazing incidence wide-angle scattering (GIWAXS) setup, has emerged as the benchmark geometry for analysing thin films of OSCs' active layers, where the incident X-ray beam is fixed to a very fixed low-angle (0.5 to 5°) with respect to the substrate normal, thus guaranteeing a maximum penetration of the X-rays through the layer [5,10,33]. The technique can be implemented in laboratory diffractometers; however, the high photon fluxes and high-brilliance X-ray beams offered by synchrotron light sources are essential, in order to produce well-defined diffraction patterns. It is worth mentioning that the outcome of a GIWAXS analysis is a 2D image allowing for the analysis of the orientation of the diffracting material with respect to the surface (so-called texture), while the Bragg–Brentano geometry provides a 1D diffractogram in which the information on the texture is missing.

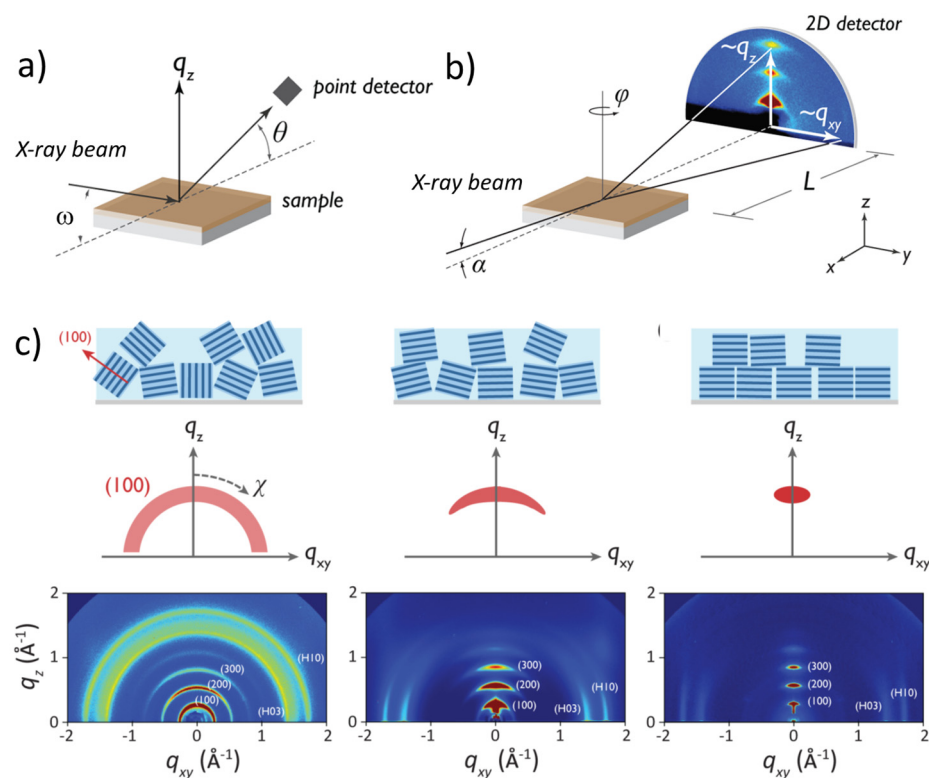


**Figure 1.** (a) Schematics of a Bragg–Brentano geometry X-ray diffraction setup. (b) Schematics of a GIWAXS geometry diffraction setup. (c) Archetypical GIWAXS images showing the correlation between diffraction peaks in the out-of-plane and in-plane directions of space and the orientation of polymer stacks. Randomly oriented crystallites would give rise to Debye diffraction rings (**left**) instead of well-defined spots (**right**). Adapted with permission from the American Chemical Society, copyright 2012 [34].

The resulting area images of GIWAXS patterns show typical diffraction planes in the out-of-plane direction (parallel to the substrate normal) and in-plane direction (perpendicular to the substrate normal). The diffraction peaks' position, shape and width can be directly related to the interplane distance (from Bragg's diffraction law), the orientation of the crystalline domains, and their size. A depiction summarising the attributes of the technique and typical scattering patterns expected for polymer-based thin films is shown in Figure 1b. The analysis of GIWAXS should first proceed with the assignment of peaks to specific reflections within the crystal lattice, if the latter is known. This is, however, usually only possible for single-crystal-like packing types, i.e., small molecules, therefore, the analysis generally consists in assigning the diffraction peaks to specific molecular or intermolecular  $d$ -spacings. The most common distances for polymers used in OSCs correspond to  $\pi$ – $\pi$  stacking spacing at  $d \approx 3.5$  Å. Additional peaks corresponding to a  $d$ -spacing in the range of 15–25 Å are often observed, corresponding to a longitudinal ordering triggered by the intermolecular interactions of alkyl chains. Once diffraction peaks are assigned, the shape of the diffraction peaks allows one to determine the orientations of diffraction planes' directions with respect to the film surface. For example, diffraction peaks near the  $q_z$  axis will be caused by planes perpendicular to the film normal, whereas those near the  $q_{xy}$  axis will be caused by planes within the film plane. This information is often used to determine whether the orientation of  $\pi$ – $\pi$  stacking is in-plane ("edge-on") or out-of-plane ("face on") (Figure 1c). Note that comprehensive details on GIWAXS can be found elsewhere [4,6,9,10,33,34].

Consequently, GIWAXS has been critical in determining the impact of crystallinity in polymer–fullerene solar cells on the  $J$ - $V$  characteristics of solar cell devices. If the GIWAXS diffraction patterns of polymer-based active layers are rather straightforward to rationalise

due to the simplified crystallisation modes of polymers, i.e., peaks corresponding to a very limited number of diffraction planes, the case of small molecules can be significantly more complex depending on their crystallisation habits. As an illustrative example, although the fullerene component (i.e., a small molecule) of polymer-based OSCs generally displays somewhat limited crystallinity in active layers when blended with polymers, in some rare cases the PCBM was shown to form a well-defined, highly ordered packing reminiscent of single-crystalline-like small molecules [35]. In these particular cases, the interplane distances corresponding to the diffraction peaks cannot be related to a direct molecular spacing. Instead, they should be related to a packing pattern from a matching X-ray diffraction single-crystal structure of PCBM (Figure 2a). In a more recent study from Lee et al., a blend of a polymer and a non-fullerene SM acceptor showed a very similar trend in which, depending on the active layer deposition conditions, the CITIQ-4F non-fullerene acceptor (NFA) can form crystallites with an extremely well-arranged pattern. Figure 2b shows the GIWAXS image of films composed of pristine CITIQ-4F, indicative of single-crystal-like packing patterns of a pure or polymorphic form, as suggested by the authors [36].

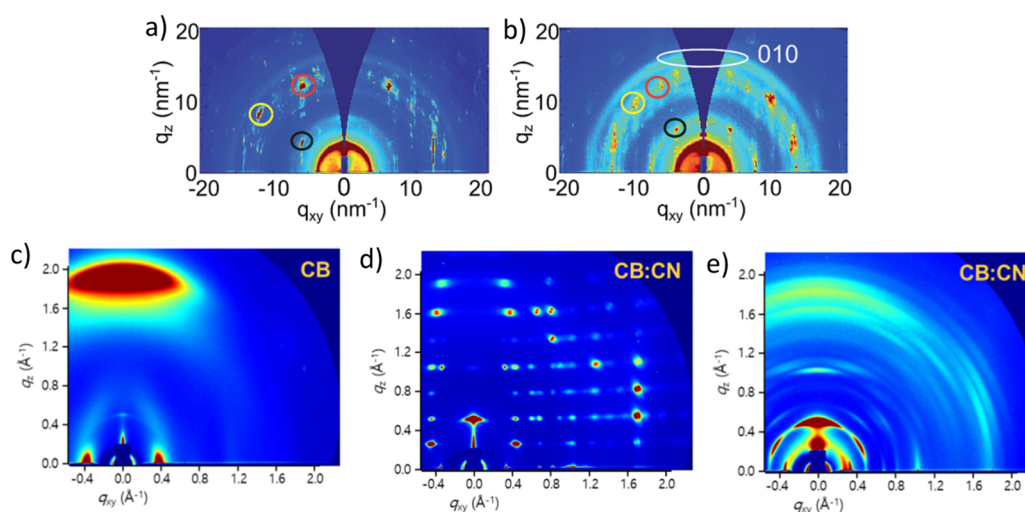


**Figure 2.** (a,b) GIWAXS diffraction patterns of P3HT:PCBM films post-treated with chlorobenzene and toluene vapours, respectively. The dominant Bragg diffraction peaks corresponding to PCBM packed in a single crystal-like fashion are marked as black, yellow and red circles. Adapted with permission from the Royal Society of Chemistry, copyright 2016 [35]. (c) GIWAXS diffraction patterns of a thin film of pristine CITIQ-4F processed from chlorobenzene; (d) GIWAXS diffraction patterns of a thin film of pristine CITIQ-4F processed from chlorobenzene containing 2% of chloronaphtalene; (e) GIWAXS diffraction patterns of a thin film of a PTB7-Th/CITIQ-4F blend processed from chlorobenzene containing 2% of chloronaphtalene. Adapted with permission from the American Chemical Society, copyright 2019 [36].

This crystallisation habit is maintained when CITIQ-4F is blended with the polymer (PTB7-th), however the texture (crystal orientation) decreases, as seen by the appearance of Debye rings instead of well-defined diffraction spots. Interestingly, this behaviour is only prevalent when a slight amount (2%) of additive is added to the processing solvent. Indeed, if pure chlorobenzene is used, CITIQ-4F forms disordered liquid-crystalline-like stacks of individual molecules, as seen by the single diffraction peak in the out-of-plane and in-plane direction in the GIWAXS image corresponding to  $d = 3.5 \text{ \AA}$  and  $d = 15.3 \text{ \AA}$  (Figure 2c). These interplane distances are straightforwardly linked to face-on p-p stacking planes and edge-on lamellar stacking. Likewise, a slight modification of CITIQ-4F chemical structure, namely adding an ether group on one of the alkyl chains, shows again a liquid-crystalline-like behaviour. In this case, the extremely ordered single crystal-like packing is not observed even using additives [36]. These experiments are capital in demonstrating

that subtle changes in either processing conditions or molecular structure can dramatically impact the crystallisation mode of SMs in thin films. Consequently, a given small molecule can adopt a single-crystal-like or liquid-crystal-like packing mode in OSC active layers. Such a shift in crystallisation habit is rather challenging to predict, however, the trend in the design of SM (D or A) consisting in adding a large number of alkyl chains to the conjugate core (far beyond the necessary amount for adequate solubility) has had a dramatic impact in shifting the crystallisation mode from a single-crystal-like to a liquid-crystalline-like. This trend has had a significant impact in reaching record PCEs in SM-BHJ OSCs, as we will expound below.

#### 4. Crystallinity and Crystalline Packing in SM-BHJ

The crystalline features in SM-BHJ are, as introduced above, more difficult to rationalise than polymer-based BHJ OSCs. The crystallisation habit of SMs in thin films, particularly in active layers composed of D/A blends, can be divided into two distinct classes: a single-crystal-like packing following one of the possible Bravais lattices, or a more disordered liquid-crystalline-like behaviour. Early SM donors were exclusively mixed with fullerene derivatives, most commonly with [6,6]-phenyl-C61-butyric acid methyl ester (PC<sub>60</sub>BM) or [6,6]-phenyl-C71-butyric acid methyl ester (PC<sub>70</sub>BM), and featured a conjugated backbone often reminiscent of polymer monomers, functionalised with alkyl chains to increase solubility [37–45]. Later SMs relied on acceptor–donor alternating units (A– $\pi$  bridge–D), which proved very effective in increasing the overall absorption coefficient of the molecule, in addition to shifting the onset of absorption towards the infrared part of the visible spectrum [46–55].

The presence of relatively short alkyl chains on the donor's structure and the rather amorphous nature of PCBM suggested consideration of the crystallinity of SMs in a single-crystalline-like fashion. As such, early studies attempted, in a rather speculative manner, to link the characteristics of PV devices, with the packing of the SM donor derived from a known X-ray crystal structure of that SM. Although the approach is sensible, it relied on the hypothetical assumption that the SM donor would adopt the identical polymorphic crystalline phase in the active layer, let alone that the active layer would be crystalline [56]. This critical limitation was partially dealt with in later studies. The active layer was characterised via conventional XRD using either Bragg–Brentano or GIWAXS configurations, and the experimental diffractograms were compared to the calculated powder diffractograms of polymorphic single-crystal structures, however, with limited accuracy [57–62]. Figure 3 shows such an attempted comparison where the scarcity of diffraction peaks in the active layers—presumably due to the very small crystallites' size, the low crystalline volume and the high degree of texture—render any comparison inaccurate. Indeed, in this early study from Bäuerle and co-workers [60], a library of oligothiophenes was reported, from which single-crystal structures were obtained of at least one polymorph for each oligothiophene derivative. The authors recorded a GIWAXS 1D diffractogram of an active layer made from a blend of a dicyanovinyl (DCV)-quaterthiophene substituted derivative (DCV4T-Me, Figure 3a) and fullerene-C60, deposited via thermal evaporation. The diffractogram shows three very broad distinct peaks, which the authors attributed to semi-amorphous C60, and to DCV4T-Me packed in an identical phase as that of the single-crystal structure obtained from DCV4T-Me (Figure 3b). Such assumptions were made from the comparison of the active layer's diffractogram (black line, Figure 3c) with a powder diffractogram of pristine C60 (blue line, Figure 3c), and with the calculated powder diffractogram of DCV4T-Me from the single crystal structure (red line). The authors assigned the highest-intensity diffraction peak of the blend to the highest-intensity calculated diffraction peak at 12° of DCV4T-Me (red line). The weak Bragg reflection at 25.95° ( $d = 3.43 \text{ \AA}$ ) in the experimental diffractogram was assigned to the calculated diffraction peak of DCV4T-Me (26.69°,  $d = 3.34 \text{ \AA}$ ). Although they assign the shift between the peaks from the experimental diffractogram and the calculated one to an increase in the unit-cell dimensions, it is evident that such comparison entails an additional set of somewhat speculative assumptions, such as a high degree of

texture (preferential orientation), and the existence of one stable polymorphic structure for DCV4T-Me. Indeed, as seen in Figure 3c, the scarcity of diffraction peaks in the active layer's diffractogram implies that the crystalline phase assignment is a more suggestive analysis rather than an accurate determination.

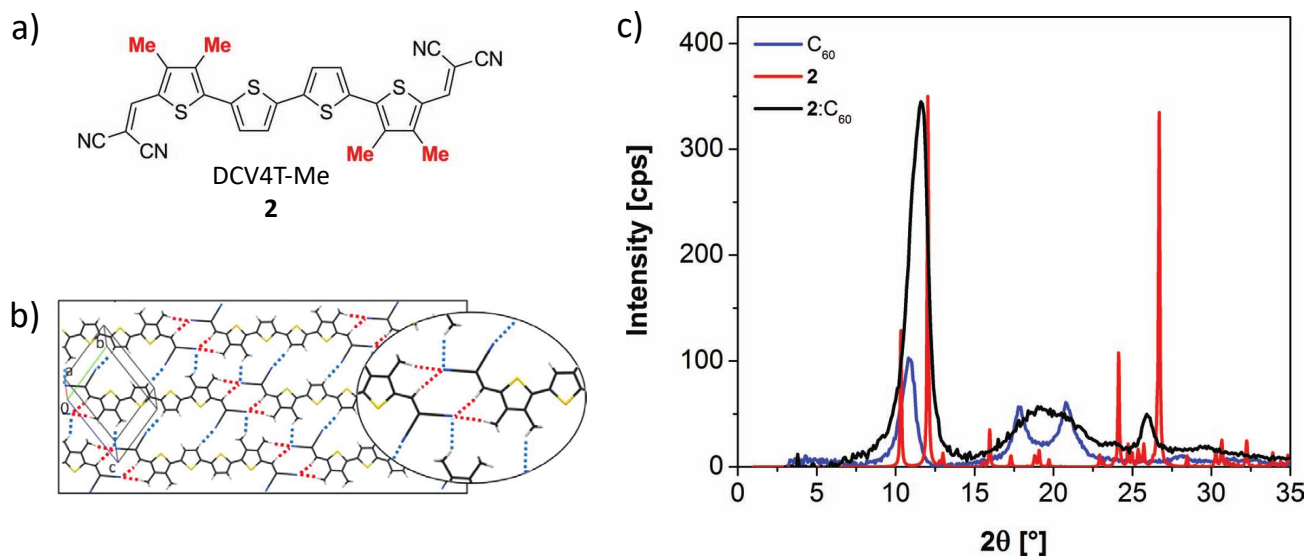


**Figure 3.** (a) Molecular structure of oligothiophene 2; (b) X-ray single-crystal structure of derivative DCV4T-Me 2 showing the molecular packing along the *ab* plane of the unit cell. Derivative 2 exhibits a layer arrangement in which molecules form rows interacting via four weak CH...NC hydrogen bonds between vinyl and methyl hydrogens and the dicyanovinyl groups (red dotted lines); (c) GIXRD diffractograms of powder  $C_{60}$  (blue line), active layer blend of 2 and  $C_{60}$ , and calculated powder diffractogram of 2 from X-ray crystal structure (b). Adapted with permission from the Wiley VCH, copyright 2012 [60].

A unique solution to the limitations expounded above was reported in a comprehensive study by our group [63], in which the crystalline phase adopted by a squaraine (SQ) donor in an active layer was accurately identified using a combination of experimental methods and powder diffraction refining methods. As such, Figure 4a shows the diffractograms (Bragg–Brentano  $\theta$ – $\theta$  configuration, out-of-plane incident beam) of spin-coated thin-film active layers of SQ:PC<sub>70</sub>BM blends. A diffraction peak at a  $2\theta$  angle of 8.01 can be seen, as well as a faint peak at  $2\theta$  angle of 16.1 in some cases. Additional GIWAXS images of the same films provided clear evidence of a highly textured film (Figure 4b). Therefore, the two peaks appearing in the diffractograms, as shown in Figure 4a, could be unambiguously attributed to reflections of the same (hkl) family of diffraction planes. More importantly, those peaks appeared to match the expected diffraction pattern of SQ packed into a P21/*n* phase with a high degree of texture, and thus with the (011) plane parallel to the substrate (Figure 4a). This identification was possible from the calculated diffractogram of SQ obtained from a single crystal structure (P21/*n* polymorphic phase) with preferential orientation along the  $\langle 011 \rangle$  direction (Figure 4a, red line).

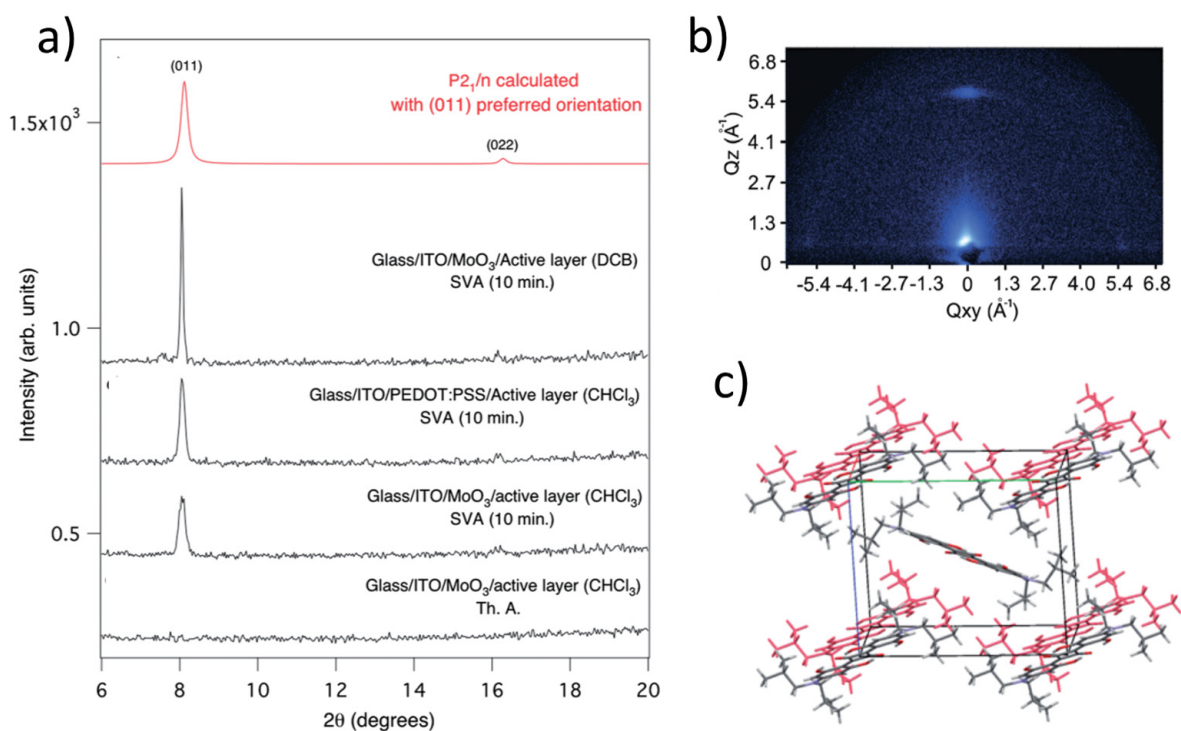


**Figure 4.** (a) Stacked diffractograms of SQ: PC<sub>70</sub>BM active layers spin-coated from different solvents and on the top of different substrates, with thermal annealing (Th. A.) or solvent vapour annealing (SVA) post-deposition treatments. (b) GIWAXS diffraction image of a typical active layer; (c) Single-crystal X-ray diffraction structure of SQ crystallised in the P21/n space group. Adapted with permission from the Royal Society of Chemistry, copyright 2014 [63].

However, similarly to the above example, the scarcity of diffraction peaks induced by the high degree of texture and the low diffraction volume limits the analysis to assumption. To circumvent this limitation, we developed an experimental turnaround consisting of recording a diffractogram of a so-called “powdered” active layers [63]. The “powdered” active layer technique consists in depositing thin films of SQ: PC<sub>70</sub>BM onto large area (>50 cm<sup>2</sup>) glass substrates using similar conditions to those used for processing active layers in OSC devices, and subsequently submitting them to solvent vapour annealing, SVA, (the annealing method used for OSCs devices fabrication of that type) for an extended period of time, in order to allow for extended crystallite growth. The resulting thin films were scraped off the glass substrate, and the solid was used for X-ray powder diffraction analysis. This somewhat simple method allowed for the acquisition of the missing information from the direct measurement of active layers, and provided an improved signal-to-noise ratio as a result of greater crystalline volume. Consequently, the appearance of several additional diffraction peaks in the diffractogram of the powdered sample confirmed the hypothesis mentioned above, whereby the experimental diffractogram appears to match, both in 2θ angle value and in relative intensity, the diffractogram calculated from the P21/n structure (Figure 5). The calculated diffractogram was further fitted to the experimental one using Rietveld refinement methods, in order to provide further quantitative evidence. Importantly, this study further demonstrated that the SQ could pack in a different space group (Pbcn) (identified using identical methodology) or a combination of the two, depending on the deposition conditions.

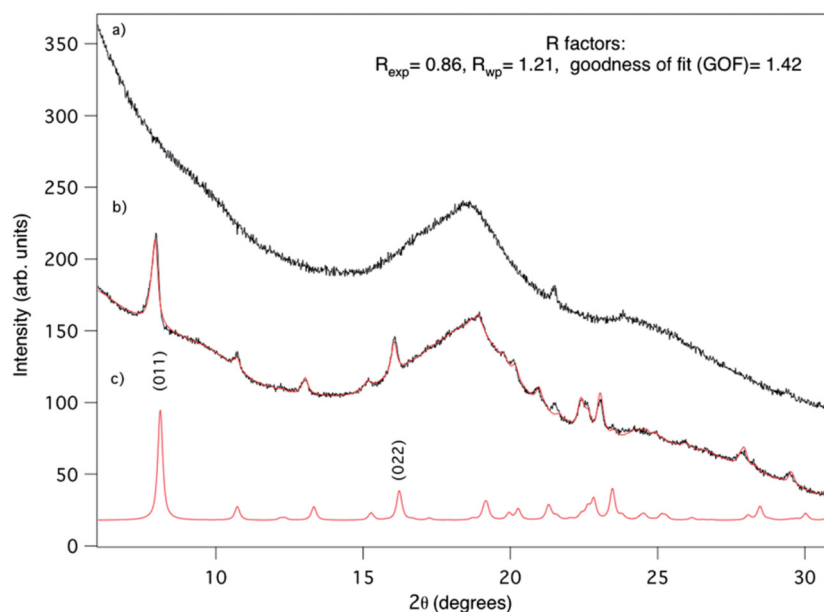


**Figure 5.** (a) Pristine PC<sub>70</sub>BM powdered layer diffractogram; (b) SQ: PC<sub>70</sub>BM “powdered” active layer diffractogram (black line) and refined diffractogram from the P21/n crystal structure of SQ (red line). The cell parameters, profile shape and scale factor were accounted for in the refinement routine, while all structural parameters (atomic positions and temperature factors) were kept constant. The Rietveld R factors provide clear evidence of structural agreement between the single crystal and the “powdered” layer; (c) calculated powder diffractogram of SQ from the P21/n X-ray single crystal structure (143 K). Adapted with permission from the Royal Society of Chemistry, copyright 2014 [63].

A subsequent extensive study from our group allowed application of the above method to a library of related donors [64]. The determination of the crystalline phase adopted by two donors in active layers of OSCs allowed an attempt of a qualitative analysis of the thermodynamics of the formation of crystallites in such active layers, in turn establishing a link between the latter parameters with the *J-V* characteristics of the devices.

According to empirical evidence, it was assumed that the crystallisation of donor molecules from the amorphous active layer would then occur via homogeneous or heterogeneous nucleation and growth mechanisms.

$$\Delta G(r) = \frac{1}{3}\pi r^3 \Delta G_V + \frac{4}{3}\pi r^3 \Delta G_E + 4\pi r^2 \gamma$$

The free energy change for a classical homogenous nucleation process implying spherical nuclei of radius  $r$  is described by equation 1. Accordingly,  $\Delta G(r)$  is seen to be dependent on three energy parameters:  $\Delta G_V$  corresponding to the bulk free energy difference of crystal formation (energy/unit volume) intrinsic to each polymorphic crystalline phase;  $\gamma$  corresponding to the interfacial energy (i.e., energy arising from the interface between the nucleus composed of pure donor molecules and the D/A amorphous matrix the nucleus is growing from); and  $\Delta G_E$  the elastic free energy change due to the strain arising from the growth of a particle in the solid matrix. The latter two energy terms act as a barrier to nucleation. The profile shape of the free energy change of the transformation for a given system is seen to proceed through a maximum value (activation energy), determining the critical nucleus size ( $r^*$ , critical radius) to be achieved for crystallite growth to become favourable (when  $d\Delta G(r)/dr = 0$ ;  $\Delta G^*$ ) [65].

Consequently, for a given active layer,  $r^*$  and  $\Delta G^*$  will be determined by the intrinsic ability of the donor molecule to arrange in a thermodynamically stable crystalline phase (maximising  $\Delta G_V$  and minimising  $\gamma$ ) in the amorphous D/A blend. The interfacial contribution to nucleus growth dominates at small nucleus sizes, while the volumetric ones ( $\Delta G_V + \Delta G_E$ ) dominate at large nucleus sizes.

In order to provide an insight into the energetics of the crystallites' growth, relative quantification of the interfacial energy  $\gamma$  of the amorphous fraction of the active layers in the early stage of crystalline growth ( $r = 0$ ) was carried out [64]. Thereafter, a quantitative analysis of the  $\Delta G_V$  contribution was derived from the free energy change of crystallisation ( $\Delta_{\text{crys}}G$ ) for derivatives **1** and **2** from the enthalpy of fusion ( $\Delta_{\text{fus}}H$ ) of pure crystalline powder samples of **1** and **2** isolated as pure P-1 and P21/c phases, respectively. The experimental values of  $\Delta_{\text{crys}}G$  show that the formation of crystallites of **2** in the P21/c phase is thermodynamically more favourable ( $(\Delta_{\text{crys}}G(2\text{-P21/c}) < \Delta_{\text{crys}}G(1\text{-P-1}))$ ) than the formation of crystallites of **1** in a P-1 phase by unit of mole. Their volumetric counterparts ( $\Delta G_V$ ) were calculated from the unit cell volume derived for each crystalline phase from the X-ray diffraction single crystal structure. We then used these values as a relative indicator to draw a hypothetical energy profile of the nucleation process (Figure 6e). The higher  $\Delta G_V$  contribution compensates for the higher interfacial energy experienced by nuclei of derivative **2** during the early step of nucleus formation. This results in  $r^*_2$  being inferior to  $r^*_1$ , and in the formation of nuclei of **1** being kinetically favoured with respect to **2** ( $\Delta G^*_1 < \Delta G^*_2$ ). This model showed good agreement with the experimental crystallisation habits of each derivative. Although limited to certain types of SM systems, the above analysis shone some light on the molecular packing of SMs and the energetics of crystallisation, when SMs (in this case, donors) adopt a well-ordered single-crystal-like packing.

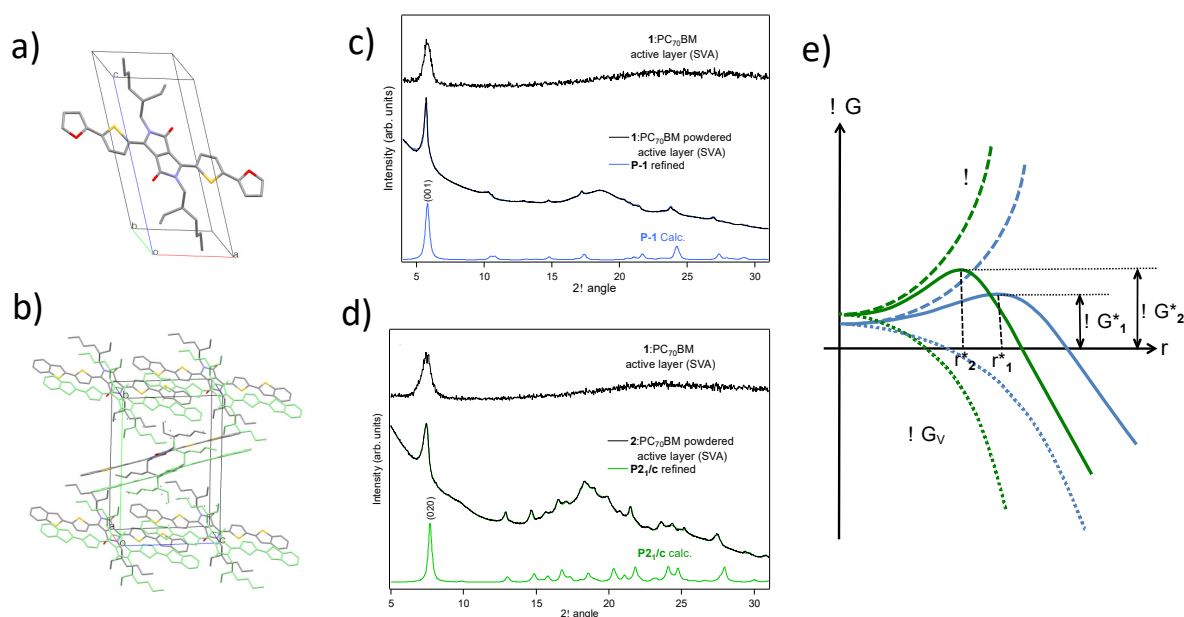


**Figure 6.** (a,b) X-ray crystal structures of molecules **1** and **2**, showing the unit cells; (c,d) Stacked diffractograms of active layers, “powdered” active layer diffractogram and superimposed refined diffractogram from the X-ray single-crystal structure, and calculated diffractogram (at 100 K) from the X-ray single-crystal structure of **1** and **2** shown in (a,b); (e) hypothetical energetic profile of donors' nucleation in active layers of derivatives **1** and **2**. Adapted with permission from Wiley VCH, copyright 2017 [64].

The advent of the DAD-type donors, particularly oligothiophene-, dithienosilole (DTS)-, benzodithiophene (BDT)-based SM donors, marked the start of a new era in SM-BHJ in a way that the crystallinity, and more importantly the packing of molecules, shifted to a liquid-crystalline-like mode. The transition between single-crystalline-like and liquid crystalline-like behaviour is well exemplified by the oligothiophenes of the DRCNT library first described by Chen and co-workers [66–70]. They consisted of a library of oligothiophenes comprised of 5 to 9 thiophenes, which pioneered the manufacture of SM-BHJ devices approaching 10% PCE. The characterisation of their typical active layers by GIWAXS

showed what appeared to be a transition between the two packing modes. The 5- and 7-thiophene analogues seem to adopt a well-defined crystalline packing of the single-crystal type or complex liquid-crystalline type, respectively, while the 6 and 9 analogues seem to form simplified  $\pi$ - $\pi$  stacks of molecules in the out-of-plane direction very reminiscent of crystalline polymers. Figure 7 shows the GIWAXS area images of DRCN5T and DRCN6T, with diffraction peaks located mainly in the out-of-plane direction for DRCN6T, while a multitude of off-meridional well-defined diffraction spots at very low  $q$  value can be seen in the data corresponding to DRCN5T. Although the authors attributed the corresponding  $d$ -spacing to a lamellar stacking distance (18–19 Å), these peaks likely correspond to a single-crystal-like packing. Interestingly, the derivatives leading to higher PCEs were those of the highly ordered nature (5- and 7-thiophene units), although the PCEs were in a rather similar range. Despite their different crystallisation modes, the hole mobility measured from the corresponding active layers was very similar for all donors (in the range of  $5 \times 10^{-4} \text{ cm}^2/\text{V}\cdot\text{s}$ ), further demonstrating that an extremely ordered crystalline packing is most probably not a determinant in obtaining devices with enhanced  $J$ - $V$  characteristics.

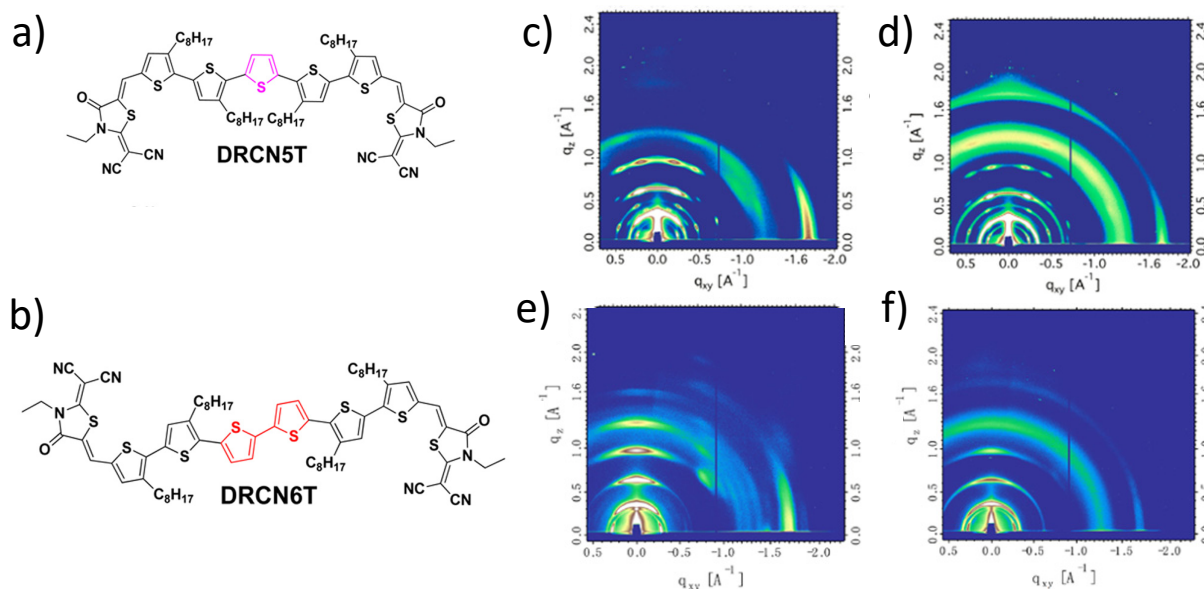


**Figure 7.** (a,b) Chemical structures of DRCN5T and DRCN6T; (c,e) GIXD patterns of pure films of DRCN5T and DRCN6T, respectively; (d,f), GIXD patterns of blend films of DRCN5T:PC<sub>71</sub>BM and DRCN6T:PC<sub>71</sub>BM, respectively. Adapted with permission from the American Chemical Society, copyright 2019 [67].

A contemporary class of SM donors to the above oligothiophene, based on the dithienosilole (DTS) core [71–79] first described by Bazan and co-workers [76], confirms the shift in crystallisation trend mentioned above. In the case of the most popular *p*-DTS (PTTh<sub>2</sub>)<sub>2</sub>, crystallisation kinetics were seen to be unusually fast, as active layers would display some degree of crystallinity directly after deposition (and therefore, some PV performance) [73]. Active layers were shown to acquire the optimum crystallinity upon processing with a small fraction of diiodooctane (DIO) additive in the processing solvent, with no further annealing required. In this particular case, the packing pattern is exclusively of the liquid-crystal type, an effect that may be enhanced by the fact that the DTS core contains alkyl chains in both the longitudinal and lateral parts of the conjugated core. This likely forces the packing towards a more disordered type, hence being favoured even under fast film drying conditions (Figure 8). The enhancement of PV properties was shown to have a clear dependency on the amount of DIO additive, and the best results were obtained when a small fraction of polystyrene was also added [80]. The additive was not shown to have an impact on the packing itself, which remains of the liquid-crystalline

type, with  $\pi$ -stacked units along the out-of-plane direction, and lamellar in the in-plane direction. However, the DIO was key in adjusting the size of the crystalline domains to an optimum value that would maximise photoinduced processes. The effect of DIO has been rationalised by carrying out *in-operando* GIWAXS studies, which showed that intermediate crystallites with different-plane spacing distances formed in the early moments of the active layer deposition, which rearrange upon the slow evaporation of the high boiling point DIO additive towards the final liquid-crystalline-type packing [77,78].

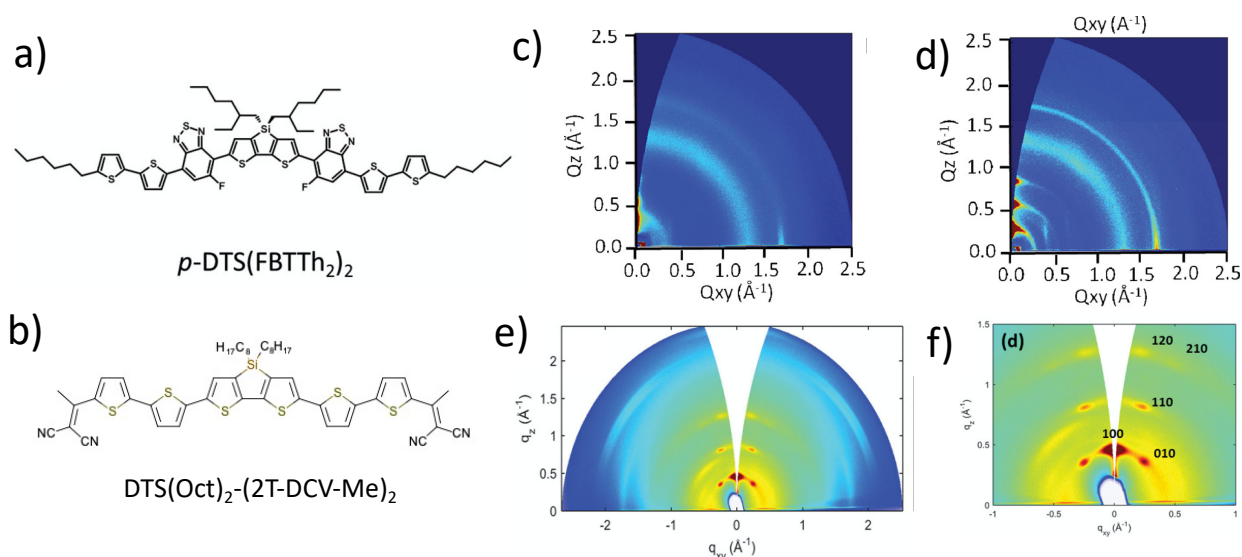


**Figure 8.** (a,b) Chemical structures of  $p$ -DTS(FBTTh<sub>2</sub>)<sub>2</sub> and DTS(Oct)<sub>2</sub>-(2T-DCV-Me)<sub>2</sub>; (c,d) GIWAXS patterns of pristine DTS(FBTTh<sub>2</sub>)<sub>2</sub> films and DTS(FBTTh<sub>2</sub>)<sub>2</sub>:PC<sub>70</sub>BM films; (e,f) GIWAXS pattern of DTS(Oct)<sub>2</sub>-(2T-DCV-Me)<sub>2</sub>:PC<sub>70</sub>BM films. Adapted with permission from Wiley VCH, copyright 2014 and 2015 [79,80].

Donors of the DTS family have been studied extensively, and it is interesting to note that at least one close derivative of the original DTS (PTTh<sub>2</sub>)<sub>2</sub> donor shows an intermediate crystalline habit in a very similar manner as the DRCNT donors described above. That is, in this particular example from Luponosov et al. [79], the DTS (Oct)<sub>2</sub>-(2T-DCV-Me)<sub>2</sub> donor, which differs from DTS (PTTh<sub>2</sub>)<sub>2</sub>, amongst other parameters, by the length of the alkyl side chains, show off-meridional symmetrical diffraction peaks at  $q$  0.47<sup>-1</sup> (Figure 8e,f). The authors suggest that this is evidence of high crystallinity and “good molecular packing” and attempted the resolution of the crystalline packing using molecular modelling tools. Here again, the experimental results demonstrate how the presence of shorter alkyl chains tips the balance towards the formation of single-crystalline-like packing rather than liquid-crystalline-like.

The ADA (or ApDpA) approach, together with the addition of an extensive amount of alkyl chains to the conjugated structure of the SM, has undoubtedly had a major impact on devices’ characteristics. The combination of the approaches culminated in the synthesis of the donors of the benzodithiophene terthiophene rhodanine (BTR) type [81–86], which resulted in record PCEs, still held to this day. Indeed, the first BTR reported by Chen and co-workers consisted of an oligothiophene structure with rhodanine end groups, where a benzodithiophene (BDT) group was intercalated in the middle of the molecular backbone [70,87,88]. Interestingly, in a later report, one of the best-performing BTR donors (simply called BTR) was clearly identified as a liquid crystalline material with a nematic phase forming above 165 °C. Additionally, and quite importantly, the authors succeeded in growing small-sized single crystals, and solved their structure using synchrotron X-ray source. Although the X-ray diffraction data were not of optimum quality, the crystal structure showed that the greatest amount of disorder is located on the alkyl chains.

The fact that the BTR molecule comprises ethylhexyl alkyl groups is an additional cause of the increased disorder, since the chirality of the tertiary carbon may imply the co-crystallisation of diastereomeric adducts. These results further confirm the hypothesis upon which the increase in alky/aromatic carbon ratio has a significant impact on shifting the crystallisation habit of SMs in active layers of OSCs from an ordered single crystalline-like mode to a more disordered liquid-crystal-like mode. Figure 9c shows the GIWAXS pattern of a typical active layer, showing a disordered nature of the molecular packing.

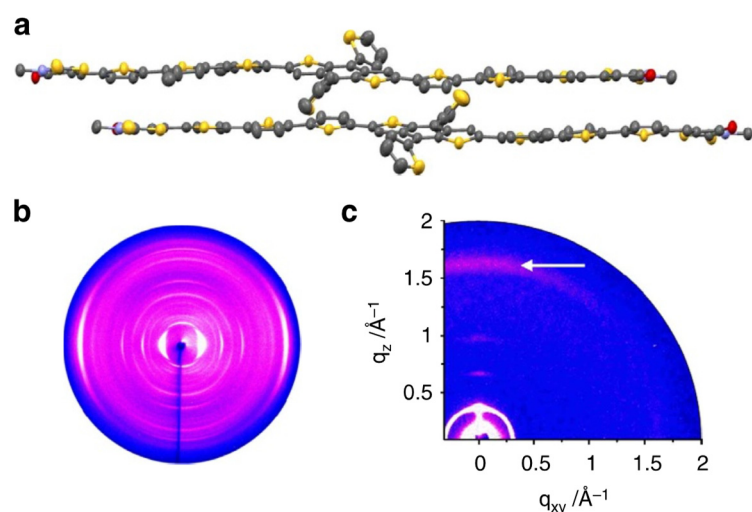


**Figure 9.** (a) X-ray diffraction single crystal structure of BTR, with the alkyl side chains omitted for clarity; (b) 2D-WAXS of BTR filament measured at 30 °C; (c) GIWAXS of spin-cast BTR thin film on silicon (p-stacking reflection is indicated by an arrow). Adapted with permission from the Nature Publishing Group, copyright 2015 [82].

## 5. Conclusions

The advent of the DA-type donors, particularly DTS, oligothiophene, BDT SM donors, marked the start of a new era in SM-BHJ in a way that the crystallinity and, more importantly, the packing of molecules shifted to a more disordered liquid-crystalline-like type. This trend is likely the result of incorporating a large number of alkyl chains in the chemical structure of the donors with respect to early SM donors. Indeed, it is remarkable that SM donors that led to efficiencies above 7% have a ratio of aliphatic to aromatic carbons often superior to one. Therefore, it is consistent with the fact that the added disorder incurred by the alkyl chains likely directs intermolecular interactions towards exclusive  $\pi$ - $\pi$  stacking and hydrophobic interactions. The disordered liquid crystalline-like packing type is consequently greatly favoured. Although the link between this increase in disorder brought about by the numerous alkyl chains and the higher PCEs is counterintuitive, it can be readily rationalised by the fact that an ordered packing type is rather difficult to achieve in such a complex medium as that of OSCs' active layers. As demonstrated in our previous study [64], the subtle thermodynamics and kinetics parameters underpinning the nucleation and growth processes are extremely difficult to control. As a consequence, the crystallites formed in such active layers often display extreme features, e.g., either too small or too large crystallites with sub-optimal anisotropic features. Liquid-crystalline-like packing SMs arise from limited types of interactions, namely p-p stacking and alkyl chain intermolecular interactions, forming much more predictable stacks of molecules. Despite the fact that disorder is more predominant in the crystalline domains, the gain in crystallisation control outcompetes the former setback to a large extent. The system is more forgiving towards the formation of homogeneously distributed (size and orientation) crystalline domains, hence the consistent increase in PCE over the years.

**Funding:** The authors thank E2S UPPA for awarding the INTERMAT international chair to E.P.

**Conflicts of Interest:** The authors declare no conflict of interest.

## References

1. Tang, C.W. Two-layer Organic Photovoltaic Cell. *Appl. Phys. Lett.* **1986**, *48*, 183–185. [[CrossRef](#)]
2. Rand, B.P.; Richter, H. (Eds.) *Organic Solar Cells: Fundamentals, Devices, and Upscaling*; Jenny Stanford Publishing: New York, NY, USA, 2014; ISBN 978-0-429-06772-3.
3. Yang, Y.; Li, G. (Eds.) *Progress in High-Efficient Solution Process Organic Photovoltaic Devices*; Topics in Applied Physics; Springer: Berlin/Heidelberg, Germany, 2015; Volume 130, ISBN 978-3-662-45508-1.
4. Salleo, A.; Kline, R.J.; DeLongchamp, D.M.; Chabynyc, M.L. Microstructural Characterization and Charge Transport in Thin Films of Conjugated Polymers. *Adv. Mater.* **2010**, *22*, 3812–3838. [[CrossRef](#)] [[PubMed](#)]
5. DeLongchamp, D.M.; Kline, R.J.; Fischer, D.A.; Richter, L.J.; Toney, M.F. Molecular Characterization of Organic Electronic Films. *Adv. Mater.* **2011**, *23*, 319–337. [[CrossRef](#)] [[PubMed](#)]
6. Mukherjee, S.; Herzog, A.A.; Zhao, D.; Wu, Q.; Yu, L.; Ade, H.; DeLongchamp, D.M.; Richter, L.J. Morphological Characterization of Fullerene and Fullerene-Free Organic Photovoltaics by Combined Real and Reciprocal Space Techniques. *J. Mater. Res.* **2017**, *32*, 1921–1934. [[CrossRef](#)]
7. Chen, W.; Nikiforov, M.P.; Darling, S.B. Morphology Characterization in Organic and Hybrid Solar Cells. *Energy Environ. Sci.* **2012**, *5*, 8045. [[CrossRef](#)]
8. Zhao, F.; Wang, C.; Zhan, X. Morphology Control in Organic Solar Cells. *Adv. Energy Mater.* **2018**, *8*, 1703147. [[CrossRef](#)]
9. Richter, L.J.; DeLongchamp, D.M.; Amassian, A. Morphology Development in Solution-Processed Functional Organic Blend Films: An In Situ Viewpoint. *Chem. Rev.* **2017**, *117*, 6332–6366. [[CrossRef](#)]
10. Xiao, Y.; Lu, X. Morphology of Organic Photovoltaic Non-Fullerene Acceptors Investigated by Grazing Incidence X-ray Scattering Techniques. *Mater. Today Nano* **2019**, *5*, 100030. [[CrossRef](#)]
11. Coropceanu, V.; Cornil, J.; da Silva Filho, D.A.; Olivier, Y.; Silbey, R.; Bredas, J.-L. Charge Transport in Organic Semiconductors. *Chem. Rev.* **2007**, *107*, 926–952. [[CrossRef](#)]
12. Bredas, J.-L.; Norton, J.E.; Cornil, J.; Coropceanu, V. Molecular Understanding of Organic Solar Cells: The Challenges. *Accounts Chem. Res.* **2009**, *42*, 1691–1699. [[CrossRef](#)]
13. Kippelen, B.; Bredas, J.-L. Organic Photovoltaics. *Energy Environ. Sci.* **2009**, *2*, 251–261. [[CrossRef](#)]
14. Clarke, T.M.; Durrant, J.R. Charge Photogeneration in Organic Solar Cells. *Chem. Rev.* **2010**, *110*, 6736–6767. [[CrossRef](#)] [[PubMed](#)]
15. Kowarik, S. Thin Film Growth Studies Using Time-Resolved x-Ray Scattering. *J. Phys.-Condes. Matter* **2017**, *29*, 043003. [[CrossRef](#)] [[PubMed](#)]
16. Liu, F.; Gu, Y.; Jung, J.W.; Jo, W.H.; Russell, T.P. On the Morphology of Polymer-Based Photovoltaics. *J. Polym. Sci. Pt. B-Polym. Phys.* **2012**, *50*, 1018–1044. [[CrossRef](#)]
17. Cranston, R.R.; Lessard, B.H. Metal Phthalocyanines: Thin-Film Formation, Microstructure, and Physical Properties. *RSC Adv.* **2021**, *11*, 21716–21737. [[CrossRef](#)] [[PubMed](#)]
18. Zeng, H.; Zhu, X.; Liang, Y.; Guo, X. Interfacial Layer Engineering for Performance Enhancement in Polymer Solar Cells. *Polymers* **2015**, *7*, 333–372. [[CrossRef](#)]
19. Wang, J.; Wang, W.; Chen, Y.; Song, L.; Huang, W. Growth and Degradation Kinetics of Organic-Inorganic Hybrid Perovskite Films Determined by In Situ Grazing-Incidence X-ray Scattering Techniques. *Small Methods* **2021**, *5*, 2100829. [[CrossRef](#)]
20. Tang, H.; Chen, H.; Yan, C.; Huang, J.; Fong, P.W.K.; Lv, J.; Hu, D.; Singh, R.; Kumar, M.; Xiao, Z.; et al. Delicate Morphology Control Triggers 14.7% Efficiency All-Small-Molecule Organic Solar Cells. *Adv. Energy Mater.* **2020**, *10*, 2001076. [[CrossRef](#)]
21. Yamamoto, T.; Komarudin, D.; Arai, M.; Lee, B.-L.; Suganuma, H.; Asakawa, N.; Inoue, Y.; Kubota, K.; Sasaki, S.; Fukuda, T.; et al. Extensive Studies on  $\pi$ -Stacking of Poly(3-Alkylthiophene-2,5-Diyl)s and Poly(4-Alkylthiazole-2,5-Diyl)s by Optical Spectroscopy, NMR Analysis, Light Scattering Analysis, and X-Ray Crystallography. *J. Am. Chem. Soc.* **1998**, *120*, 2047–2058. [[CrossRef](#)]
22. Tremel, K.; Ludwigs, S. Morphology of P3HT in Thin Films in Relation to Optical and Electrical Properties. In *P3HT Revisited – From Molecular Scale to Solar Cell Devices*; Ludwigs, S., Ed.; Advances in Polymer Science; Springer: Berlin/Heidelberg, Germany, 2014; Volume 265, pp. 39–82. ISBN 978-3-662-45144-1.
23. Vanlaeke, P.; Swinnen, A.; Haeldermans, I.; Vanhoyland, G.; Aernouts, T.; Cheyens, D.; Deibel, C.; D’Haen, J.; Heremans, P.; Poortmans, J.; et al. P3HT/PCBM Bulk Heterojunction Solar Cells: Relation between Morphology and Electro-Optical Characteristics. *Solar Energy Mater. Solar Cells* **2006**, *90*, 2150–2158. [[CrossRef](#)]
24. Chirvase, D.; Parisi, J.; Hummelen, J.C.; Dyakonov, V. Influence of Nanomorphology on the Photovoltaic Action of Polymer-Fullerene Composites. *Nanotechnology* **2004**, *15*, 1317–1323. [[CrossRef](#)]
25. Padinger, F.; Rittberger, R.S.; Sariciftci, N.S. Effects of Postproduction Treatment on Plastic Solar Cells. *Adv. Funct. Mater.* **2003**, *13*, 85–88. [[CrossRef](#)]
26. Erb, T.; Zhokhavets, U.; Gobsch, G.; Raleva, S.; Stühn, B.; Schilinsky, P.; Waldauf, C.; Brabec, C.J. Correlation Between Structural and Optical Properties of Composite Polymer/Fullerene Films for Organic Solar Cells. *Adv. Funct. Mater.* **2005**, *15*, 1193–1196. [[CrossRef](#)]

27. Kim, Y.; Choulis, S.A.; Nelson, J.; Bradley, D.D.C.; Cook, S.; Durrant, J.R. Composition and Annealing Effects in Polythiophene/Fullerene Solar Cells. *J. Mater. Sci.* **2005**, *40*, 1371–1376. [[CrossRef](#)]
28. Spoltore, D.; Oosterbaan, W.D.; Khelifi, S.; Clifford, J.N.; Viterisi, A.; Palomares, E.; Burgelman, M.; Lutsen, L.; Vanderzande, D.; Manca, J. Effect of Polymer Crystallinity in P3HT:PCBM Solar Cells on Band Gap Trap States and Apparent Recombination Order. *Adv. Energy Mater.* **2013**, *3*, 466–471. [[CrossRef](#)]
29. Auremma, F.; De Rosa, C.; Corradini, P. Solid Mesophases in Semicrystalline Polymers: Structural Analysis by Diffraction-Techniques. In *Interphases and Mesophases in Polymer Crystallization II*; Allegra, G., Ed.; Advances in Polymer Science; Springer: Berlin/Heidelberg, Germany, 2005; Volume 181, pp. 1–74, ISBN 978-3-540-25344-0.
30. Blinov, L.M. *Structure and Properties of Liquid Crystals*; Springer: Dordrecht, The Netherlands, 2011; ISBN 978-90-481-8828-4.
31. Hammond, C. *The Basics of Crystallography and Diffraction*, 4th ed.; International Union of Crystallography Texts on Crystallography; Oxford University Press: Oxford, UK, 2015; ISBN 978-0-19-873867-1.
32. Guinebretiere, R. *X-ray Diffraction by Polycrystalline Materials*; ISTE: London, UK; Newport Beach, CA, USA, 2007; ISBN 978-1-905209-21-7.
33. Mahmood, A.; Wang, J. A Review of Grazing Incidence Small- and Wide-Angle X-Ray Scattering Techniques for Exploring the Film Morphology of Organic Solar Cells. *Sol. RRL* **2020**, *4*, 2000337. [[CrossRef](#)]
34. Rivnay, J.; Mannsfeld, S.C.B.; Miller, C.E.; Salleo, A.; Toney, M.F. Quantitative Determination of Organic Semiconductor Microstructure from the Molecular to Device Scale. *Chem. Rev.* **2012**, *112*, 5488–5519. [[CrossRef](#)]
35. Wang, W.; Guo, S.; Herzig, E.M.; Sarkar, K.; Schindler, M.; Magerl, D.; Philipp, M.; Perlich, J.; Müller-Buschbaum, P. Investigation of Morphological Degradation of P3HT:PCBM Bulk Heterojunction Films Exposed to Long-Term Host Solvent Vapor. *J. Mater. Chem. A* **2016**, *4*, 3743–3753. [[CrossRef](#)]
36. Lee, J.; Ko, S.-J.; Lee, H.; Huang, J.; Zhu, Z.; Seifrid, M.; Vollbrecht, J.; Brus, V.V.; Karki, A.; Wang, H.; et al. Side-Chain Engineering of Nonfullerene Acceptors for Near-Infrared Organic Photodetectors and Photovoltaics. *ACS Energy Lett.* **2019**, *4*, 1401–1409. [[CrossRef](#)]
37. Roncali, J.; Leriche, P.; Blanchard, P. Molecular Materials for Organic Photovoltaics: Small Is Beautiful. *Adv. Mater.* **2014**, *26*, 3821–3838. [[CrossRef](#)]
38. Kesters, J.; Verstappen, P.; Kelchtermans, M.; Lutsen, L.; Vanderzande, D.; Maes, W. Porphyrin-Based Bulk Heterojunction Organic Photovoltaics: The Rise of the Colors of Life. *Adv. Energy Mater.* **2015**, *5*, 1500218. [[CrossRef](#)]
39. Walker, B.; Kim, C.; Nguyen, T.-Q. Small Molecule Solution-Processed Bulk Heterojunction Solar Cells. *Chem. Mater.* **2011**, *23*, 470–482. [[CrossRef](#)]
40. Riede, M.; Mueller, T.; Tress, W.; Schueppel, R.; Leo, K. Small-Molecule Solar Cells—Status and Perspectives. *Nanotechnology* **2008**, *19*, 424001. [[CrossRef](#)]
41. Chen, Y.; Wan, X.; Long, G. High Performance Photovoltaic Applications Using Solution-Processed Small Molecules. *Acc. Chem. Res.* **2013**, *46*, 2645–2655. [[CrossRef](#)] [[PubMed](#)]
42. Koerner, C.; Ziehlke, H.; Fitzner, R.; Riede, M.; Mishra, A.; Bäuerle, P.; Leo, K. Dicyanovinylene-Substituted Oligothiophenes for Organic Solar Cells. In *Elementary Processes in Organic Photovoltaics*; Leo, K., Ed.; Advances in Polymer Science; Springer International Publishing: Cham, Switzerland, 2017; Volume 272, pp. 51–75, ISBN 978-3-319-28336-4.
43. Li, M.; Ni, W.; Wan, X.; Zhang, Q.; Kan, B.; Chen, Y. Benzo[1,2-b:4,5-b']Dithiophene (BDT)-Based Small Molecules for Solution Processed Organic Solar Cells. *J. Mater. Chem. A* **2015**, *3*, 4765–4776. [[CrossRef](#)]
44. Malyskiy, V.; Simon, J.-J.; Patrone, L.; Raimundo, J.-M. Thiophene-Based Push–Pull Chromophores for Small Molecule Organic Solar Cells (SMOSCs). *RSC Adv.* **2015**, *5*, 354–397. [[CrossRef](#)]
45. Ryan, J.W.; Palomares, E. Photo-Induced Charge Carrier Recombination Kinetics in Small Molecule Organic Solar Cells and the Influence of Film Nanomorphology. *Adv. Energy Mater.* **2017**, *7*, 1601509. [[CrossRef](#)]
46. Wang, Z.; Zhu, L.; Shuai, Z.; Wei, Z. A- $\pi$ -D- $\pi$ -A Electron-Donating Small Molecules for Solution-Processed Organic Solar Cells: A Review. *Macromol. Rapid Commun.* **2017**, *38*, 1700470. [[CrossRef](#)]
47. Tang, H.; Yan, C.; Huang, J.; Kan, Z.; Xiao, Z.; Sun, K.; Li, G.; Lu, S. Benzodithiophene-Based Small-Molecule Donors for Next-Generation All-Small-Molecule Organic Photovoltaics. *Matter* **2020**, *3*, 1403–1432. [[CrossRef](#)]
48. Coughlin, J.E.; Henson, Z.B.; Welch, G.C.; Bazan, G.C. Design and Synthesis of Molecular Donors for Solution-Processed High-Efficiency Organic Solar Cells. *Acc. Chem. Res.* **2014**, *47*, 257–270. [[CrossRef](#)]
49. Chen, H.; Tang, H.; Hu, D.; Xiao, Y.; Fu, J.; Lv, J.; Yu, Q.; Xiao, Z.; Lu, X.; Hu, H.; et al. Design of All-Small-Molecule Organic Solar Cells Approaching 14% Efficiency via Isometric Terminal Alkyl Chain Engineering. *Energies* **2021**, *14*, 2505. [[CrossRef](#)]
50. Kini, G.P.; Jeon, S.J.; Moon, D.K. Design Principles and Synergistic Effects of Chlorination on a Conjugated Backbone for Efficient Organic Photovoltaics: A Critical Review. *Adv. Mater.* **2020**, *32*, 1906175. [[CrossRef](#)]
51. Ilmi, R.; Haque, A.; Khan, M.S. High Efficiency Small Molecule-Based Donor Materials for Organic Solar Cells. *Organic Electronics* **2018**, *58*, 53–62. [[CrossRef](#)]
52. Kan, B.; Kan, Y.; Zuo, L.; Shi, X.; Gao, K. Recent Progress on all-small Molecule Organic Solar Cells Using small-molecule Nonfullerene Acceptors. *InfoMat* **2021**, *3*, 175–200. [[CrossRef](#)]
53. Collins, S.D.; Ran, N.A.; Heiber, M.C.; Nguyen, T.-Q. Small Is Powerful: Recent Progress in Solution-Processed Small Molecule Solar Cells. *Adv. Energy Mater.* **2017**, *7*, 1602242. [[CrossRef](#)]

54. Kumar, C.V.; Cabau, L.; Koukaras, E.N.; Viterisi, A.; Sharma, G.D.; Palomares, E. Solution Processed Organic Solar Cells Based on A–D–D'–D–A Small Molecule with Benzo[1,2-b:4,5-B']Dithiophene Donor (D') Unit, Cyclopentadithiophene Donor (D) and Ethylrhodanine Acceptor Unit Having 6% Light to Energy Conversion Efficiency. *J. Mater. Chem. A* **2015**, *3*, 4892–4902. [CrossRef]
55. Kumar, C.V.; Cabau, L.; Viterisi, A.; Biswas, S.; Sharma, G.D.; Palomares, E. Solvent Annealing Control of Bulk Heterojunction Organic Solar Cells with 6.6% Efficiency Based on a Benzodithiophene Donor Core and Dicyano Acceptor Units. *J. Phys. Chem. C* **2015**, *119*, 20871–20879. [CrossRef]
56. Montcada, N.F.; Pelado, B.; Viterisi, A.; Alberio, J.; Coro, J.; de la Cruz, P.; Langa, F.; Palomares, E. High Open Circuit Voltage in Efficient Thiophene-Based Small Molecule Solution Processed Organic Solar Cells. *Organic Electron.* **2013**, *14*, 2826–2832. [CrossRef]
57. Viterisi, A.; Gispert-Guirado, F.; Ryan, J.W.; Palomares, E. Formation of Highly Crystalline and Texturized Donor Domains in DPP(TBFu)<sub>2</sub>:PC71BM SM-BHJ Devices via Solvent Vapour Annealing: Implications for Device Function. *J. Mater. Chem.* **2012**, *22*, 15175. [CrossRef]
58. Liu, J.; Zhang, Y.; Phan, H.; Sharenko, A.; Moonsin, P.; Walker, B.; Promarak, V.; Nguyen, T.-Q. Effects of Stereoisomerism on the Crystallization Behavior and Optoelectrical Properties of Conjugated Molecules. *Adv. Mater.* **2013**, *25*, 3645–3650. [CrossRef]
59. Kim, C.; Liu, J.; Lin, J.; Tamayo, A.B.; Walker, B.; Wu, G.; Nguyen, T.-Q. Influence of Structural Variation on the Solid-State Properties of Diketopyrrolopyrrole-Based Oligophenyleneethiophenes: Single-Crystal Structures, Thermal Properties, Optical Bandgaps, Energy Levels, Film Morphology, and Hole Mobility. *Chem. Mater.* **2012**, *24*, 1699–1709. [CrossRef]
60. Fitzner, R.; Elschner, C.; Weil, M.; Uhrich, C.; Körner, C.; Riede, M.; Leo, K.; Pfeiffer, M.; Reinold, E.; Mena-Osteritz, E.; et al. Interrelation between Crystal Packing and Small-Molecule Organic Solar Cell Performance. *Adv. Mater.* **2012**, *24*, 675–680. [CrossRef] [PubMed]
61. Wei, G.; Wang, S.; Sun, K.; Thompson, M.E.; Forrest, S.R. Solvent-Annealed Crystalline Squaraine: PC70BM (1:6) Solar Cells. *Adv. Energy Mater.* **2011**, *1*, 184–187. [CrossRef]
62. Wei, G.; Wang, S.; Renshaw, K.; Thompson, M.E.; Forrest, S.R. Solution-Processed Squaraine Bulk Heterojunction Photovoltaic Cells. *ACS Nano* **2010**, *4*, 1927–1934. [CrossRef] [PubMed]
63. Viterisi, A.; Montcada, N.F.; Kumar, C.V.; Gispert-Guirado, F.; Martin, E.; Escudero, E.; Palomares, E. Unambiguous Determination of Molecular Packing in Crystalline Donor Domains of Small Molecule Solution Processed Solar Cell Devices Using Routine X-Ray Diffraction Techniques. *J. Mater. Chem. A* **2014**, *2*, 3536. [CrossRef]
64. Fernandez, D.; Viterisi, A.; Challuri, V.; Ryan, J.W.; Martinez-Ferrero, E.; Gispert-Guirado, F.; Martinez, M.; Escudero, E.; Stenta, C.; Marsal, L.F.; et al. Understanding the Limiting Factors of Solvent-Annealed Small-Molecule Bulk-Heterojunction Organic Solar Cells from a Chemical Perspective. *ChemSusChem* **2017**, *10*, 3118–3134. [CrossRef] [PubMed]
65. Kinetics of Materials | Wiley. Available online: <https://www.wiley.com/en-us/Kinetics+of+Materials-p-9780471246893> (accessed on 30 March 2022).
66. Zhang, X.; Ding, Y.; Wan, X.; Ke, X.; Li, C.; Chen, Y. A Novel Acceptor with a *N,N*-Dialkyl Thieno[3',2':2,3]Indolo[7,6-g]Thieno[3,2-b]Indole (TITI) Core for Organic Solar Cells with a High Fill Factor of 0.75. *Chem. Commun.* **2020**, *56*, 751–753. [CrossRef]
67. Kan, B.; Li, M.; Zhang, Q.; Liu, F.; Wan, X.; Wang, Y.; Ni, W.; Long, G.; Yang, X.; Feng, H.; et al. A Series of Simple Oligomer-like Small Molecules Based on Oligothiophenes for Solution-Processed Solar Cells with High Efficiency. *J. Am. Chem. Soc.* **2015**, *137*, 3886–3893. [CrossRef]
68. Zhang, Q.; Wang, Y.; Kan, B.; Wan, X.; Liu, F.; Ni, W.; Feng, H.; Russell, T.P.; Chen, Y. A Solution-Processed High Performance Organic Solar Cell Using a Small Molecule with the Thieno[3,2-b]Thiophene Central Unit. *Chem. Commun.* **2015**, *51*, 15268–15271. [CrossRef]
69. Zhang, Q.; Kan, B.; Liu, F.; Long, G.; Wan, X.; Chen, X.; Zuo, Y.; Ni, W.; Zhang, H.; Li, M.; et al. Small-Molecule Solar Cells with Efficiency over 9%. *Nature Photon* **2015**, *9*, 35–41. [CrossRef]
70. Kan, B.; Zhang, Q.; Li, M.; Wan, X.; Ni, W.; Long, G.; Wang, Y.; Yang, X.; Feng, H.; Chen, Y. Solution-Processed Organic Solar Cells Based on Dialkylthiol-Substituted Benzodithiophene Unit with Efficiency near 10%. *J. Am. Chem. Soc.* **2014**, *136*, 15529–15532. [CrossRef] [PubMed]
71. Zhou, J.; Wan, X.; Liu, Y.; Long, G.; Wang, F.; Li, Z.; Zuo, Y.; Li, C.; Chen, Y. A Planar Small Molecule with Dithienosilole Core for High Efficiency Solution-Processed Organic Photovoltaic Cells. *Chem. Mater.* **2011**, *23*, 4666–4668. [CrossRef]
72. Gupta, V.; Lai, L.F.; Datt, R.; Chand, S.; Heeger, A.J.; Bazan, G.C.; Singh, S.P. Dithienogermole-Based Solution-Processed Molecular Solar Cells with Efficiency over 9%. *Chem. Commun.* **2016**, *52*, 8596–8599. [CrossRef] [PubMed]
73. Love, J.A.; Proctor, C.M.; Liu, J.; Takacs, C.J.; Sharenko, A.; van der Poll, T.S.; Heeger, A.J.; Bazan, G.C.; Nguyen, T.-Q. Film Morphology of High Efficiency Solution-Processed Small-Molecule Solar Cells. *Adv. Funct. Mater.* **2013**, *23*, 5019–5026. [CrossRef]
74. Kyaw, A.K.K.; Wang, D.H.; Gupta, V.; Leong, W.L.; Ke, L.; Bazan, G.C.; Heeger, A.J. Intensity Dependence of Current–Voltage Characteristics and Recombination in High-Efficiency Solution-Processed Small-Molecule Solar Cells. *ACS Nano* **2013**, *7*, 4569–4577. [CrossRef]
75. Mukherjee, S.; Proctor, C.M.; Bazan, G.C.; Nguyen, T.-Q.; Ade, H. Significance of Average Domain Purity and Mixed Domains on the Photovoltaic Performance of High-Efficiency Solution-Processed Small-Molecule BHJ Solar Cells. *Adv. Energy Mater.* **2015**, *5*, 1500877. [CrossRef]
76. Sun, Y.; Welch, G.C.; Leong, W.L.; Takacs, C.J.; Bazan, G.C.; Heeger, A.J. Solution-Processed Small-Molecule Solar Cells with 6.7% Efficiency. *Nat. Mater* **2012**, *11*, 44–48. [CrossRef]

77. Perez, L.A.; Chou, K.W.; Love, J.A.; van der Poll, T.S.; Smilgies, D.-M.; Nguyen, T.-Q.; Kramer, E.J.; Amassian, A.; Bazan, G.C. Solvent Additive Effects on Small Molecule Crystallization in Bulk Heterojunction Solar Cells Probed During Spin Casting. *Adv. Mater.* **2013**, *25*, 6380–6384. [[CrossRef](#)]
78. Abdelsamie, M.; Treat, N.D.; Zhao, K.; McDowell, C.; Burgers, M.A.; Li, R.; Smilgies, D.-M.; Stingelin, N.; Bazan, G.C.; Amassian, A. Toward Additive-Free Small-Molecule Organic Solar Cells: Roles of the Donor Crystallization Pathway and Dynamics. *Adv. Mater.* **2015**, *27*, 7285–7292. [[CrossRef](#)]
79. Min, J.; Luponosov, Y.N.; Gasparini, N.; Richter, M.; Bakirov, A.V.; Shcherbina, M.A.; Chvalun, S.N.; Grodd, L.; Grigorian, S.; Ameri, T.; et al. Effects of Alkyl Terminal Chains on Morphology, Charge Generation, Transport, and Recombination Mechanisms in Solution-Processed Small Molecule Bulk Heterojunction Solar Cells. *Adv. Energy Mater.* **2015**, *5*, 1500386. [[CrossRef](#)]
80. Huang, Y.; Wen, W.; Mukherjee, S.; Ade, H.; Kramer, E.J.; Bazan, G.C. High-Molecular-Weight Insulating Polymers Can Improve the Performance of Molecular Solar Cells. *Adv. Mater.* **2014**, *26*, 4168–4172. [[CrossRef](#)] [[PubMed](#)]
81. Xu, C.; Chen, H.; Zhao, Z.; Gao, J.; Ma, X.; Lu, S.; Zhang, X.; Xiao, Z.; Zhang, F. 14.46% Efficiency Small Molecule Organic Photovoltaics Enabled by the Well Trade-off between Phase Separation and Photon Harvesting. *J. Energy Chem.* **2021**, *57*, 610–617. [[CrossRef](#)]
82. Sun, K.; Xiao, Z.; Lu, S.; Zajaczkowski, W.; Pisula, W.; Hanssen, E.; White, J.M.; Williamson, R.M.; Subbiah, J.; Ouyang, J.; et al. A Molecular Nematic Liquid Crystalline Material for High-Performance Organic Photovoltaics. *Nat. Commun.* **2015**, *6*, 6013. [[CrossRef](#)] [[PubMed](#)]
83. Chen, H.; Hu, D.; Yang, Q.; Gao, J.; Fu, J.; Yang, K.; He, H.; Chen, S.; Kan, Z.; Duan, T.; et al. All-Small-Molecule Organic Solar Cells with an Ordered Liquid Crystalline Donor. *Joule* **2019**, *3*, 3034–3047. [[CrossRef](#)]
84. Subbiah, J.; Lee, C.J.; Mitchell, V.D.; Jones, D.J. Effect of Side-Chain Modification on the Active Layer Morphology and Photovoltaic Performance of Liquid Crystalline Molecular Materials. *ACS Appl. Mater. Interfaces* **2021**, *13*, 1086–1093. [[CrossRef](#)] [[PubMed](#)]
85. Xiao, L.; Yan, C.; Li, Z.; Zhong, W.; Tan, W.; Liu, Y.; Liu, F.; Peng, X.; Min, Y. Morphology Evolution Induced by Sequential Annealing Enabling Enhanced Efficiency in All-Small Molecule Solar Cells. *ACS Appl. Energy Mater.* **2021**, *4*, 4234–4241. [[CrossRef](#)]
86. Shan, T.; Ding, K.; Yu, L.; Wang, X.; Zhang, Y.; Zheng, X.; Chen, C.; Peng, Q.; Zhong, H. Spatially Orthogonal 2D Sidechains Optimize Morphology in All-Small-Molecule Organic Solar Cells. *Adv. Funct. Mater.* **2021**, *31*, 2100750. [[CrossRef](#)]
87. Zhou, J.; Wan, X.; Liu, Y.; Zuo, Y.; Li, Z.; He, G.; Long, G.; Ni, W.; Li, C.; Su, X.; et al. Small Molecules Based on Benzo[1,2-b:4,5-B']Dithiophene Unit for High-Performance Solution-Processed Organic Solar Cells. *J. Am. Chem. Soc.* **2012**, *134*, 16345–16351. [[CrossRef](#)]
88. Zhou, J.; Zuo, Y.; Wan, X.; Long, G.; Zhang, Q.; Ni, W.; Liu, Y.; Li, Z.; He, G.; Li, C.; et al. Solution-Processed and High-Performance Organic Solar Cells Using Small Molecules with a Benzodithiophene Unit. *J. Am. Chem. Soc.* **2013**, *135*, 8484–8487. [[CrossRef](#)]